

## SUB-ASTRONOMICAL UNIT STRUCTURE OF THE NEAR-INFRARED EMISSION FROM AB AURIGAE

R. MILLAN-GABET AND F. P. SCHLOERB

Department of Physics and Astronomy, University of Massachusetts, Amherst, MA 01003; rmillang@comet.phast.umass.edu

W. A. TRAUB

Harvard-Smithsonian Center for Astrophysics, 60 Garden Street, Cambridge, MA 02138

F. MALBET AND J. P. BERGER

Laboratoire d'Astrophysique, Observatoire de Grenoble, Grenoble Cedex 9, F-38041, France

AND

J. D. BREGMAN

NASA Ames Research Center, Moffet Field, CA 94035

Received 1998 December 15; accepted 1999 January 14; published 1999 January 28

### ABSTRACT

We present near-infrared, long-baseline, interferometric observations of AB Aurigae, a well-known Herbig Ae/Be star, obtained with the Infrared Optical Telescope Array. The near-infrared emission from this source has been spatially resolved for the first time, and the observations indicate a characteristic diameter of 5 mas for the emission, corresponding to 0.7 AU at the distance of AB Aur. The data appear to be most consistent with models in which the circumstellar material around AB Aurigae lies in a flattened structure with a central large hole or optically thin region of radius about 0.3 AU.

*Subject headings:* circumstellar matter — infrared: stars — stars: emission-line, Be — stars: individual (AB Aurigae) — stars: pre-main-sequence — techniques: interferometric

### 1. INTRODUCTION

The Herbig Ae/Be stars are generally understood to be pre-main-sequence stars of intermediate mass ( $1.5 < M_*/M_\odot < 10$ ) (Herbig 1960; Strom et al. 1972). Some workers (Hillenbrand et al. 1992; Lada & Adams 1992; Natta et al. 1993; Corcoran & Ray 1998) have suggested that Herbig Ae/Be stars, like their lower mass T Tauri counterparts, are surrounded by circumstellar disks. Modeling of the spectral energy distribution (SED) has shown that accretion disk models with relatively high accretion rates ( $6 \times 10^{-7} < \dot{M} < 8 \times 10^{-5} M_\odot \text{ yr}^{-1}$ ) may be able to reproduce the observations provided that a hole exists in the inner region of the disk (Hillenbrand et al. 1992). Imaging studies of the outer regions of Herbig Ae/Be stars at millimeter wavelengths (Mannings & Sargent 1997) have also shown evidence of an elongated structure and kinematic gradients that might be expected to surround an inner disk of material.

Accretion disk models can explain some, but not all, of the properties of Herbig Ae/Be stars, and the nature of the circumstellar material has remained controversial. One problem is that the hole in the inner region of the disk that is required to match the SED is difficult to understand in the context of realistic accretion disk models. Hartmann, Kenyon, & Calvet (1993) have pointed out that such a system would require either that infalling material would have to pile up at the inner edge of the disk or that ~90% of the accretion energy would have to escape detection in the SED. Another difficulty is found in studies of the profiles of forbidden line emission from Herbig Ae/Be stars. In T Tauri stars, these lines appear blueshifted because of the presence of an optically thick disk around the star that hides the redshifted component of the stellar wind, but in Herbig Ae/Be stars, Böhm & Catala (1994) find that the lines are symmetric and inconsistent with such a model (see, however, Corcoran & Ray 1997 for opposite conclusions based on similar data). Thus, alternative ideas, such as those involving a symmetric dust envelope (Berrilli et al. 1992; Hartmann et al. 1993; Miroshnichenko, Ivezić, & Elitzur 1997; Pezzuto,

Strafella, & Lorenzetti 1997), have been proposed to explain the excess infrared (IR) emission from the Herbig Ae/Be stars.

Clearly, one way to make progress on this important question is to obtain observations of the near-IR emission with sufficient angular resolution to resolve the structure around the star. In this Letter, we present long-baseline, interferometric observations of the near-IR emission around AB Aurigae, a well-studied example of a Herbig Ae/Be star; these observations have successfully resolved the circumstellar material at sub-astronomical unit resolution and permitted the characteristic size, shape, and surface brightness of the region to be estimated. In § 2 of this Letter, we describe our observations and data reduction method. In § 3, we present our visibility curves and their interpretation in terms of extended dust emission around the central star. In § 4, we discuss the implications of our results for the leading models of the circumstellar matter around Herbig Ae/Be stars.

### 2. OBSERVATIONAL PROCEDURE AND DATA REDUCTION

#### 2.1. Observations

The Infrared Optical Telescope Array (IOTA) is a Michelson stellar interferometer (Traub 1998) located on Mount Hopkins, Arizona. The observations in this Letter were obtained in the near-IR *H* and *K'* bands, using our newly developed NICMOS3 camera as the fringe detector (Millan-Gabet et al. 1999). The maximum baseline length at IOTA is 38 m, corresponding to a nominal resolution (FWHM of point source response) of  $\lambda/2B \sim 4$  and 6 mas in the *H* ( $\lambda_0 = 1.65 \mu\text{m}$ ,  $\Delta\lambda = 0.30 \mu\text{m}$ ) and *K'* ( $\lambda_0 = 2.16 \mu\text{m}$ ,  $\Delta\lambda = 0.32 \mu\text{m}$ ) bands, respectively.

Interference fringes are formed by scanning the delay between the two interferometer arms through the white-light position. An *observation* consists of 500 consecutive interference fringe sweeps obtained during an interval of about 2 minutes. Observations of the target object are interleaved with observations of an unresolved object in order to calibrate the instrumental response of the interferometer and the effect of at-

TABLE 1  
VISIBILITY DATA

Band	Baseline ( $M\lambda$ )	Visibility <sup>a</sup> (%)	rms (%)	Observation Number	Number of Nights
$H$ .....	12.8	$78 \pm 2$	5.7	10	2
	23.1	$56 \pm 1$	3.7	14	3
$K'$ .....	9.6	$85 \pm 1$	1.0	3	2
	17.3	$69 \pm 3$	5.6	6	1

<sup>a</sup> The visibility uncertainties are the error in the mean,  $\text{rms}/(N_{\text{obs}} - 1)^{1/2}$ .

atmospheric seeing on the data. The visual magnitudes ( $V$ ), spectral types, angular separations ( $d$ ) from AB Aur, and the approximate angular diameter ( $\theta$ ) of the calibrator stars used for the AB Aur ( $V = 7.1$ ,  $H = 5.1$ ,  $K = 4.4$ , A0) observations are as follows: HR 1343 ( $V = 4.93$ , G8 III,  $d = 9^{\circ}0$ ,  $\theta = 1.5$  mas), HR 2219 ( $V = 4.35$ , G8.5 IIIb,  $d = 17^{\circ}9$ ,  $\theta = 2.0$  mas), and HR 1626 ( $V = 6.14$ , K0 II–III,  $d = 2^{\circ}5$ ,  $\theta = 1.0$  mas).

## 2.2. Visibility Results

Each individual fringe is fitted in the time domain, using the instrument’s theoretical point-source response as a template, in order to determine the fringe visibility. From the 500 independent visibility values in each observation, we estimate the source visibility using a physical model of the visibility distribution function. Our model incorporates the source visibility, the signal-to-noise ratios of the individual visibilities, and the effect of random tilts between the wave fronts from the two telescopes that arise from atmospheric seeing. We find that seeing effects can strongly bias the estimate of visibility from a distribution. Hereafter, we use the term “visibility” to mean the estimated source visibility, with the atmospheric seeing and instrumental biases removed. A detailed description of the model and estimation procedure will be presented in a future paper. We note that a simpler method for the estimation of visibilities, such as the mean of the 500 independent values, results in a larger scatter when nights of different seeing conditions are included; however, the main results of this Letter would be essentially unchanged.

Observations of AB Aur were made throughout the time period 1997 October–1998 March using two baselines, the longest IOTA baseline of 38 m, which is oriented approximately north-northeast, and a 21 m north-south baseline. For these baselines, the projected baseline length on AB Aur varied by less than 1% over the hour angle range observed (approximately  $-1$  to  $3$  hr). Moreover, measurements made on the longest baseline show no evidence of a variation in the visibility as the interferometer baseline rotated with respect to the source. For these reasons, we have considered all observations of AB Aur on a given baseline to be independent estimates of the same visibility value, and we have used the observed distribution of measurements about the mean value for each baseline to assess the overall measurement error.

The average values of visibility for the  $H$  and  $K'$  bands are presented in Table 1. We find that the distribution of visibility estimates about the mean is characterized by an rms value of approximately 5%, which therefore would represent the typical error in a single AB Aur measurement due to all sources. We attribute the bulk of this uncertainty to residual calibration errors, since this value exceeds the expected error due to random noise in the initial fringe-fitting process, which is on the order of 1%. Photometric variations of the star itself, which are common in pre-main-sequence objects, may also contribute

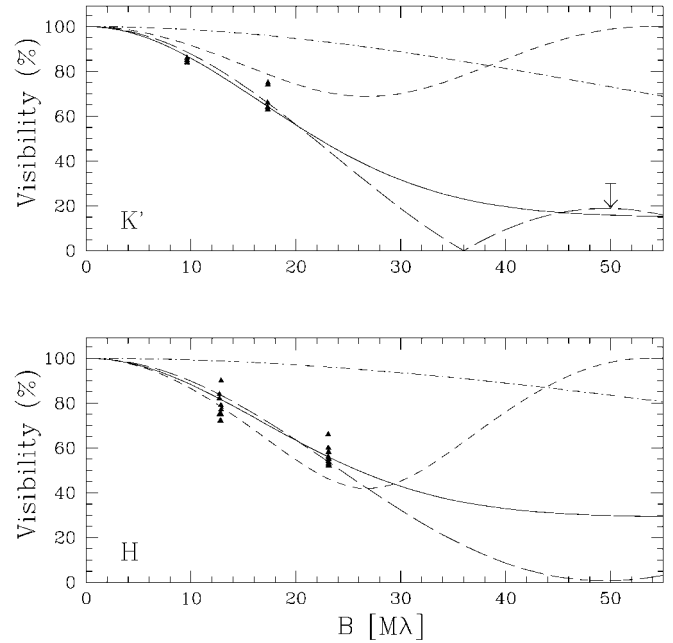


FIG. 1.—Visibility of AB Aur as a function of baseline length data and comparison with models of the source brightness distribution described in the text. The bottom panel shows the  $H$ -band data, and the top panel shows the  $K'$ -band data. The  $K'$  panel also shows the upper limit corresponding to the PTI observation. The models are plotted as follows: Gaussian (solid lines); ring (long-dashed lines); binary (dashed lines); and accretion disk (dash-dotted lines). The Gaussian and ring models provide an acceptable fit to the visibility data.

to the observed dispersion. However, we note that a change in the near-IR magnitudes of 0.1 would result only in a 1% change in the visibility, and therefore this effect is not believed to dominate the residual night-to-night variations observed.

Even considering a 5% calibration error source, the data demonstrate clearly that the AB Aur system is resolved. Moreover, we may use this error estimate to place an upper limit on the variation of visibility with changing baseline position angle on the source. We find that the visibility varies by less than 5% over the range of position angles observed ( $-10^{\circ}$  to  $20^{\circ}$ ). This result is important since it suggests that the source is not highly elongated. The data are shown in Figure 1, where we also include a visibility upper limit of 30% at a longer baseline (110 m) set by the nondetection of fringes in  $K$ -band observations at the Palomar Testbed Interferometer (PTI) (Berger 1998).

## 3. SOURCE MODEL

### 3.1. Near-IR Excess due to Circumstellar Material

The near-IR flux from the AB Aur system arises from both circumstellar material and AB Aur itself, and both contributions need to be taken into account in order to interpret the visibility data. To estimate the stellar and circumstellar near-IR fluxes, we use the  $V$ ,  $R$ ,  $I$ ,  $H$ , and  $K$  photometry data tabulated by Hillenbrand et al. (1992), and we adopt an extinction to the star ( $A_V = 0.5$ ) and an effective temperature of 10,000 K (van den Ancker et al. 1997). By adjusting the stellar radius to match the dereddened  $V$ ,  $R$ , and  $I$  fluxes, we derive  $R_* = 2.32 R_{\odot}$ .

Using this model to represent the stellar contribution, we calculate the  $H$  and  $K$  stellar fluxes, and we deduce the excess fluxes due to circumstellar emission by subtracting from the dereddened total fluxes. We find that the excess flux represents

about 71% of the total in  $H$  and 84% in  $K$ . From the  $H$  and  $K$  excess fluxes (6.79 and 9.48 Jy, respectively), we derive a color temperature of 1865 K for the circumstellar material.

### 3.2. Visibility Models

The decrease in visibility with baseline length in Figure 1 indicates that the source is resolved by the interferometer and permits an estimate of the effective size of the near-IR-emitting region to be made. However, the size estimate depends significantly on the details of the source brightness distribution, and therefore we have made estimates for three plausible models of the source brightness. Each of the three models has two components, with the emission from the central star arising from a point source ( $R_*$  derived above results in an angular diameter at 144 pc of 0.15 mas and is therefore assumed unresolved) and the excess near-IR emission contributed by either (1) a circularly symmetric Gaussian brightness distribution; (2) a uniformly bright circular ring; or (3) a companion star modeled as a second point source. The peak surface brightness in the Gaussian model is set by the requirement that the flux of this component match the near-IR excess flux, and therefore, in this case, there is no a priori constraint on the actual intensity. For the ring model, however, we have constrained the extended component to have a surface brightness equivalent to that of a blackbody at the color temperature derived from the observed excess at  $H$  and  $K$ . Thus, for all models, the only fitted parameter is the size of the extended component or the binary separation. Finally, we note that in all cases, except the binary case, the model is circularly symmetric so as to be consistent with our limit on the variation of visibility with baseline position angle.

Table 2 summarizes the detailed features of each of the models and the results of fits of the models to the visibility data. The visibility functions for the best-fitting models are displayed in Figure 1 along with the data. A formal model fit to each individual color yields a somewhat larger size for the emission in the  $H$  band than for the emission in the  $K'$  band. However, within the errors, we find that the derived sizes in the  $H$  and  $K'$  bands are consistent with a single value. Thus, Table 2 contains the results of fits to the entire data set (excluding the PTI upper limit).

In addition to the descriptive models presented in Table 2, it is also possible to compute visibility predictions for physical source models considered by previous workers. Thus, in Figure 1, we present a model calculation for an accretion disk model (cf. Hillenbrand et al. 1992) for comparison with the data. For this example, we have adopted a  $T \propto r^{-3/4}$  falloff for the temperature in the disk, and we determine the size of the hole and the temperature at the inner edge of the hole from the near-IR excess observed at  $H$  and  $K$ . The values thus obtained are 0.68 mas (0.10 AU) for the hole diameter and 3026 K for the brightness temperature at this position. These values are similar to those derived for AB Aur by Hillenbrand et al. (1992) from their fit to the entire infrared excess. Since the fluxes completely determine the model in this case, there are no free parameters left to fit to the visibility data, and therefore Figure 1 simply shows the visibility function that is predicted by the model. It is clear that this model does not agree with the visibility data.

## 4. DISCUSSION OF MODELS

Previous high angular resolution observations of AB Aur, via millimeter-wave interferometry (Mannings & Sargent 1997), mid-infrared imaging (Marsh et al. 1995), and near-IR speckle interferometry (Leinert, Richichi, & Haas 1997), have

TABLE 2  
SUMMARY OF SOURCE MODELS

Parameter	Gaussian <sup>a</sup>	Ring <sup>b</sup>	Binary <sup>c</sup>
Size (mas) .....	4.66 ± 0.11	4.74 ± 0.09	3.85 ± 0.41
Size (AU) .....	0.67 ± 0.02	0.68 ± 0.01	0.55 ± 0.06
$H$ -band $T_b$ (K) .....	1318	1865	1865
$K'$ -band $T_b$ (K) .....	1200	1865	1865
rms (%) .....	5.6	5.7	9.9

<sup>a</sup> Gaussian model: the size is FWHM;  $T_b$  is the brightness temperature at the Gaussian peak. The observed brightness temperatures are consistent with optically thin emission from the source (see text).

<sup>b</sup> Ring model: the size is the inner diameter of ring; the outer diameter is adjusted to match the flux in the  $H$  and  $K$  bands, yielding a ratio of outer/inner diameter of 1.14. The ring is considered to be optically thick, and  $T_b$  is constrained to be the color temperature of the infrared excess.

<sup>c</sup> Binary model: the size is the angular separation of the primary and secondary (the companion is assumed unresolved) projected along the baseline direction;  $T_b$  is constrained to be the color temperature of the infrared excess.

all failed to resolve the inner  $\sim 1$  AU where the near-IR emission arises. However, in this work, the use of a long-baseline, near-IR interferometer has enabled the system to be resolved for the first time. It is clear from Figure 1 and from consideration of the residual rms values that the Gaussian and ring models provide an adequate fit to the data, while the binary model and accretion disk models do not.

### 4.1. Binary Model

As noted by Hartmann et al. (1993), one plausible model for the infrared excess in Herbig Ae/Be stars is a companion embedded in a thick envelope of dust. In this case, the companion is invisible in the optical parts of the spectrum and appears as an infrared source because of the absorption of starlight by the dust envelope and the subsequent reradiation at cooler temperatures. The binary model shown in Table 2 and Figure 1 does not fit the visibility data as well as the other models presented. Moreover, our limit on the variation in visibility with baseline position angle constrains the possible orientation of the binary system. Considering the most complete set of data, the  $H$ -band observations on the longest IOTA baseline, we find that the binary position angle would have to lie within the range of  $0^\circ$ – $10^\circ$  in order to be consistent with the 5% limit on the visibility variation. These special constraints make this model a less attractive explanation than the others presented here.

### 4.2. Accretion Disk Model

Figure 1 shows the visibility function that is predicted by the accretion disk model, and it is clear that this model does not agree with the visibility data. Indeed, we find that it is not possible to match simultaneously the visibility data and the infrared excess for any temperature power-law model in the range  $T \propto r^{-0.5}$ – $r^{-1.0}$ . Finally, we find that a general property of the visibility function of such models is that the effective size of the disk at the  $H$  band is smaller than that in the  $K'$  band, in contradiction to the observation that both data sets are consistent with the same effective size. Thus, it appears that the accretion disk models commonly used to explain the source SED are not consistent with our interferometric measurements.

### 4.3. Ring Model

The choice of a ring to describe the emission was originally motivated by a desire to find a structure that is consistent with the effective size measured by the interferometer and with

thermal emission at the color temperature derived from the  $H$  and  $K$  excess. It is interesting to note that this descriptive model of the emission would result from a physical accretion disk model in the event that the temperature gradient in the disk were very steep (approximately  $r^{-8}$ ) at its inner edge, so that the  $H$  and  $K$  emission arise from essentially the same radius. Thus, if an accretion disk provides the physical explanation of the overall infrared excess in AB Aur, then the inner structure of the disk is quite different from the generally accepted range of power-law models, with essentially the entire near-infrared excess originating from a narrow ring around the star.

Another consideration about accretion disk and ring models is that the visibility data are consistent with circularly symmetric emission and that the lack of any strong variation in visibility places constraints on the inclination of the disk. For example, for an inclined disk oriented along a position angle of  $79^\circ$  to be consistent with millimeter-wave (Mannings & Sargent 1997) and mid-IR images (Marsh et al. 1995), the observed symmetry implies an inclination of less than  $45^\circ$  for the disk. The  $76^\circ$  inclination derived by Mannings & Sargent (1997) from their millimeter-wave maps falls well outside this allowed range and suggests that the disk structure in the inner 1 AU does not follow a simple extrapolation from the apparent behavior of the source at hundreds of astronomical units from the star.

#### 4.4. Gaussian Model

The descriptive Gaussian model provides a good match to the visibility data but needs to be interpreted in physical terms in order to provide further information about the nature of the source. The brightness temperature that is derived from the model fit falls well below the 1865 K color temperature implied by the  $H - K$  color. One possible interpretation of this observation is that the near-IR emission is optically thin. In such a case, the observed color temperature would depend on both the physical temperature and the emission properties of the grains in the source.

With the assumption that circumstellar material is optically thin and that its optical depth varies with wavelength according to the standard interstellar extinction curve (which implies  $A_H/A_K = \tau_H/\tau_K = 1.67$ ), it is possible to derive the grain temperature ( $T$ ) and near-IR optical depth ( $\tau$ ) from the surface brightness temperature ( $T_b$ ) measured with the interferometer.

The observed intensity at frequency  $\nu$  is  $I_\nu = B_\nu(T_b) = B_\nu(T)(1 - e^{-\tau})$ , where  $B_\nu(T)$  is the Planck function. Using the values of the brightness temperature derived for the Gaussian model (see Table 2), we estimate a grain temperature of 1434 K and an optical depth in the  $H$  band of 0.9. This temperature compares favorably with the temperature of blackbody grains at a distance of 0.3 AU from AB Aur, suggesting that grains heated by starlight might be able to account for the observed near-IR excess. However, the required near-IR optical depth implies a visible extinction toward the star of approximately 3 mag, which is inconsistent with the observed line-of-sight extinction to AB Aur. Thus, according to this model, the distribution of dust around the star could not be spherically symmetric but would likely need to be flattened in a disk.

#### 4.5. Conclusions

Our interferometric observations appear to be inconsistent with classical accretion disk models, such as those proposed by Hillenbrand et al. (1992). However, they do appear to be consistent with a flattened distribution of dust around the star in which the inner  $\sim 0.3$  AU radius is either empty of material (e.g., the ring model) or optically thin in the near-IR (the Gaussian model). The large hole inferred from the ring model provides an attractive explanation of the symmetric emission lines that are observed toward the star (Böhm & Catala 1994). This fact is less well accounted for by the simple, optically thin, Gaussian model presented here, which would still contain a significant optical depth of dust. However, more complex mass distributions that would allow the full emission-line region to be observed would certainly be permitted by the observations. Finally, we note that our limit on the variation of visibility with baseline position angle places a strong constraint on the orientation and/or thickness of the flattened dust distribution. If the material in the inner region lies in a thin disk, then it cannot be highly inclined to the observer.

Observations and instrument development at the IOTA are supported by funding from the SAO and the University of Massachusetts; work at IOTA is also funded by NASA (NSG-7176 to Harvard University and NAG5-4900 to SAO) and the NSF (ASR90-21181 to IOTA consortium members and AST 95-28129 to the University of Massachusetts).

#### REFERENCES

- Berger, J. P. 1998, Ph.D. thesis, Univ. Joseph Fourier de Grenoble, France  
 Berrilli, F., Corciulo, G., Ingrosso, G., Lorenzetti, D., Nisini, B., & Strafella, F. 1992, *ApJ*, 398, 2254  
 Böhm, T., & Catala, C. 1994, *A&A*, 290, 167  
 Corcoran, M., & Ray, T. P. 1997, *A&A*, 321, 189  
 ———. 1998, *A&A*, 331, 147  
 Hartmann, L., Kenyon, S. J., & Calvet, N. 1993, *ApJ*, 407, 219  
 Herbig, G. H. 1960, *ApJS*, 4, 337  
 Hillenbrand, L. A., Strom, S. E., Vrba, F. J., & Keene, J. 1992, *ApJ*, 397, 613  
 Lada, C. J., & Adams, F. C. 1992, *ApJ*, 393, 278  
 Leinert, C., Richichi, A., & Haas, M. 1997, *A&A*, 318, 472  
 Mannings, V., & Sargent, A. I. 1997, *ApJ*, 490, 792  
 Marsh, K. A., Van Cleve, J. E., Mahoney, M. J., Hayward, T. L., & Houck, J. R. 1995, *ApJ*, 451, 777  
 Millan-Gabet, R., Schloerb, F. P., Traub, W. A., & Carleton, N. P. 1999, *PASP*, 111, 238  
 Miroshnichenko, A., Ivezić, Ž., & Elitzur, M. 1997, *ApJ*, 475, L41  
 Natta, A., Palla, F., Butner, H. M., Evans, N. J., & Harvey, P. M. 1993, *ApJ*, 406, 674  
 Pezzuto, S., Strafella, F., & Lorenzetti, D. 1997, *ApJ*, 485, 290  
 Strom, S. E., Strom, K. M., Yost, J., Carrasco, L., & Grasdalen, G. 1972, *ApJ*, 173, 353  
 Traub, W. A. 1998, *Proc. SPIE*, 3350, 848  
 van den Ancker, M. E., Thé, P. S., Tjin, H. R. E., Djie, A., Catala, C., de Winter, D., Blondel, P. F. C., & Waters, L. B. F. M. 1997, *ApJ*, 324, L33